

Article

Optoelectronics and Transport Phenomena in $\text{Rb}_2\text{InBiX}_6$ ($X = \text{Cl}, \text{Br}$) Compounds for Renewable Energy Applications: A DFT Insight

Debidatta Behera  and Sanat Kumar Mukherjee * 

Department of Physics, Birla Institute of Technology, Mesra, Ranchi 835215, India

* Correspondence: sanat_aphy@yahoo.co.in

Abstract: In this study, we used the FP-LAPW technique based on density functional theory applied in WIEN2k code to examine the structural, electronic, elastic, and thermoelectric properties of cubic double perovskite $\text{Rb}_2\text{InBiX}_6$ ($X = \text{Cl}, \text{Br}$) compounds. The structural stability was confirmed from the tolerance factor, formation energy, and phonon dispersion. The exchange-correlation potentials LDA, GGA, mBJ, and HSE were used to estimate the electronic properties. According to the band structure computed band gap using mBJ, the HSE are 1.61 eV, 1.81 eV for $\text{Rb}_2\text{InBiCl}_6$ and 1.22 eV, 1.32 eV for $\text{Rb}_2\text{InBiBr}_6$ compounds, respectively. The mechanical stability of the materials under examination were reflected by the calculated elastic constants. The estimated bulk modulus-to-shear modulus ratios for $\text{Rb}_2\text{InBiX}_6$ ($X = \text{Cl}, \text{Br}$) are 2.13 and 3.65, respectively. This indicates that the examined compounds were ductile in nature. The optical properties in terms of real and imaginary dielectric functions, refractive index, and absorption coefficient were computed, indicating that they might be employed in optoelectronic and photovoltaic applications. In the temperature range 200–800 K, the electrical conductivity, Seebeck coefficient, thermal conductivity, and power factor (PF) were analysed. Relatively high PFs of about $2.7 \times 10^{10} \text{ W/K}^2 \text{ ms}$ and $3.1 \times 10^{10} \text{ W/K}^2 \text{ ms}$ were obtained for $\text{Rb}_2\text{InBiX}_6$ ($X = \text{Cl}, \text{Br}$) suggesting that these compounds are viable for usage in thermoelectric devices. Both the compounds showed strong absorption patterns and excellent PF signifying that these are suitable materials for photovoltaic and thermoelectric applications.

Keywords: thermoelectricity; double perovskite; band gap; optical properties; power factor



Citation: Behera, D.; Mukherjee, S.K. Optoelectronics and Transport Phenomena in $\text{Rb}_2\text{InBiX}_6$ ($X = \text{Cl}, \text{Br}$) Compounds for Renewable Energy Applications: A DFT Insight. *Chemistry* **2022**, *4*, 1044–1059. <https://doi.org/10.3390/chemistry4030071>

Academic Editor: Andrea Peluso

Received: 16 August 2022

Accepted: 13 September 2022

Published: 15 September 2022

Publisher's Note: MDPI stays neutral with regard to jurisdictional claims in published maps and institutional affiliations.



Copyright: © 2022 by the authors. Licensee MDPI, Basel, Switzerland. This article is an open access article distributed under the terms and conditions of the Creative Commons Attribution (CC BY) license (<https://creativecommons.org/licenses/by/4.0/>).

1. Introduction

The need for energy has significantly increased in recent years, which has accelerated efforts to identify non-fossil fuel and non-conventional energy sources. It leads to a shift in global attention towards renewable energy sources [1,2]. Thermoelectricity is a promising method of creating renewable energy that allows for the efficient utilization of waste heat through the direct conversion of thermal and electrical energies [3–5]. The efficiency of thermoelectric (TE) material is evaluated by the figure of merit (ZT), as $ZT = (S^2\sigma T)/(\kappa_e + \kappa_l)$, where S is the Seebeck coefficient, σ is electrical conductivity, T is the absolute temperature, and κ_e, κ_l is electronic and lattice contributions to the thermal conductivity [1,6]. Achieving an optimum ZT requires high thermoelectric power factor ($S^2\sigma$) and minimum thermal conductivity (κ). Using a basic understanding of thermoelectricity, researchers are working on enhancing thermoelectric power factor ($S^2\sigma$) and reducing thermal conductivity (κ) [7–9]. Energy filtering, rational structure/lattice imperfection designs that include dislocations, and point defects are considered to minimize κ by improving multi-wavelength phonon scattering as well as having been considered to increase $S^2\sigma$. As a result, new and novel thermoelectric materials with the best ZT are emerging [9]. However, in recent decades, perovskite-based compounds have received interest and are found to exhibit exceptional ZT. Because they offer diverse physical, chemical and catalytic properties, many scientists and researchers are interested in these compounds. Simple

perovskites (ABX_3) have a cubic crystal structure and belong to the space group Fm-3m (225). Due to the fact that the A-site cation has 12 coordination numbers, it creates a 12-fold octahedron geometry with its neighbours [10]. The B-site cation forms octahedral geometry by interacting with its surrounding anions. In addition to normal perovskites, double perovskites have drawn a lot of attention due to their extraordinary potential for modern applications. The double perovskite has the formula $A_2BB'X_6$, in which the B- and B'-site are occupied by transition/non-transition cations, and the A-site is filled by a rare-earth or alkaline-earth metal and X belongs to oxides or halides. The extraordinary properties of halide-based double perovskites, such as their electrical, optical, thermoelectric, and superconducting capabilities, have aroused the interest of researchers in a wide range of technologically significant disciplines as well as applied and basic domains of material research [11–14]. According to literature, the monovalent (M^+) and trivalent (M^{3+}) ions can be used to replace Pb^{2+} ions in ABX_3 to produce lead-free, novel, halide-based double perovskite $A_2M^+M^{3+}X_6$ compounds [15–19]. Recently, a number of novel double perovskite compounds were reported. In this context, A as K, Cs, Rb, M^+ cation as Cu, Ag, In and M^{3+} cation as Bi, Sb and X as Cl, Br, I compounds were well reported, emphasizing their optoelectronics and transport properties [20–28]. Due to the extraordinary importance of the Bi^{3+} and Sb^{3+} ions, numerous inorganic double perovskite compounds based on them have undergone extensive research [29]. Using ab initio calculations, Savory et al. investigated the electronic characteristics of double perovskites Cs_2MBiX_6 ($M = Ag, Bi$ and $X = Cl, Br, I$) [30]. These compounds, according to the findings, could be utilised in high-efficiency solar cells. Xiao et al. employed density functional theory (DFT) simulations to analyse the thermodynamic stability of $Cs_2AgBiBr_6$ [31]. The two lead-free double perovskite compounds $Cs_2AgBiBr_6$ and $Cs_2AgBiCl_6$ were synthesized by Filip et al. and were found to be efficient for visible absorption semiconductors [32]. Wei et al. synthesized double perovskite, $Cs_2AgSbBr_6$ single crystals using the hydrothermal method. XRD and UV VIS data suggested that the material has a cubic phase (Fm-3m) with a lattice parameter of 11.15 Å and an indirect band gap of 1.64 eV [33]. According to several theoretical and experimental studies, the double perovskite compound $Cs_2AgInCl_6$ is appropriate for a wide range of solar and thermoelectric device applications [34,35]. Although the material has a reasonable band gap energy under normal circumstances, it should be noted that due to an indirect band gap, the material behaves differently when exposed to sunlight. Mukhtar et al. investigated A_2KGA_6 ($A = Cs, Rb$) double perovskite compounds that possess a direct band gap of 1.81 eV, 1.85 eV. The PF for Cs_2KGA_6 is $2.89 \times 10^{11} \text{ W/K}^2 \text{ ms}$ and for Rb_2KGA_6 is $3.17 \times 10^{11} \text{ W/K}^2 \text{ ms}$ at 800 K, respectively [36]. Saeed et al. studied Cs_2AgCrX_6 ($X = Cl, Br, \text{ and } I$) compounds exhibiting strong carrier mobility between the valence band (VB) and conduction band (CB). Because of its high electrical conductivity and Seebeck coefficient, Cs_2AgCrI_6 is a potential thermoelectric material [37]. Iqbal et al. studied Rb_2AlInX_6 ($X = Cl, Br, I$) double perovskites and revealed their stability using a phonon dispersion study. The calculated power factor at 300 K is $2.43 \times 10^{11} \text{ W/K}^2 \text{ ms}$, $2.53 \times 10^{11} \text{ W/K}^2 \text{ ms}$, and $2.63 \times 10^{11} \text{ W/K}^2 \text{ ms}$ for Rb_2AlInX_6 ($X = Cl, Br, I$), which indicates that these compounds are suitable for thermoelectric device applications [38]. While substantial studies on Cs-based halide double perovskite compounds have been conducted, there has been fewer reports on Rb-based halide double perovskite compounds both experimentally and theoretically [39]. The Rb with an atomic radius ~ 303 pm possesses identical physical and chemical properties to that of Cs (atomic radius ~ 363 pm). According to Saliba et al., Rb incorporation in a perovskite-based solar cell can enhance its stability and photovoltaic performance [40]. However, from a literature survey, Rb-based halide double perovskite Rb_2InBiX_6 ($X = Cl, Br$) compounds have not been intensively investigated. Motivated by the above, in this study, first-principles calculations were used to study the structural, elastic, electronic, optical, and thermoelectric properties of the Rb_2InBiX_6 ($X = Cl, Br$) compounds. The manuscript is divided into three sections. Section 1 discusses the introduction, Section 2 gives a thorough explanation of the computational approach

employed in the current study, and Section 3 discusses the results and conclusions that were found to be extremely important in the field of scientific research today.

2. Computational Method

The structural, mechanical, and transport characteristics of $\text{Rb}_2\text{InBiX}_6$ ($X = \text{Cl}, \text{Br}$) compounds were calculated employing a WIEN2k code [41] programme employing Perdew-Burke-Ernzerhof (PBE) techniques within density functional theory (DFT) [42]. The modified Becke-Johnson (mBJ) exchange approximation was also taken into consideration in order to achieve more precise electrical and optical properties [43]. Electronic and optical properties were computed using the PBE+mBJ potential. The region is separated into two parts in the FP-LAPW approach [44]: the interstitial region and the un-overlapping muffin tin (MT) spheres. The MT radii for Rb, In, Bi, Cl, and Br atoms were calculated to be 2.35, 1.80, 1.77, 2.01, and 1.64 atomic units (a.u.). In the unit cell, the smallest muffin tin radius is $R_{\text{MT}}, K_{\text{max}} \times R_{\text{MT}} = 8$. $G_{\text{max}} = 12 \text{ au}^{-1}$ was set as the maximum Fourier expansion of charge density. A total of 1000 k-points were employed, together with the $10 \times 10 \times 10$ grid, to integrate the reciprocal space of the irreducible Brillouin zone. The total convergence threshold energy 10^{-5} Ry was used to complete the self-consistent computations. We employed the IRelast package [45] to study the mechanical properties of investigated $\text{Rb}_2\text{InBiX}_6$ ($X = \text{Cl}, \text{Br}$) compounds. Additionally using VASP (Vienna Ab-initio Simulation Package) software [46], the band structure (HSE) phonon dispersion studies were performed. We utilized the BoltzTraP [47] algorithm to determine the thermoelectric characteristics. A fine grid mesh ($46 \times 46 \times 46$) was considered for calculation of transport properties.

3. Result and Discussion

3.1. Structural Properties

Figure 1 shows the crystal structure of $\text{Rb}_2\text{InBiX}_6$ ($X = \text{Cl}, \text{Br}$) compounds, which displays cubic face-centered atomic configuration with space group Fm-3m (225) [48]. The constituent atoms Rb, In, Bi, and X are located at (0.25, 0.25, 0.25), (0.5, 0.5, 0.5), (0, 0, 0), and (y, 0, 0), respectively ($y = 0.247$) [49,50]. We used the PBE-GGA functional to optimize the structural parameters for both compounds. Table 1 shows the structural parameters and bond length of all the atoms for the studied $\text{Rb}_2\text{InBiX}_6$ ($X = \text{Cl}, \text{Br}$) compounds. It is noticed that for the examined compounds, the lattice constant increases as the anion switches from Cl to Br because Br has a larger ionic radius than Cl. The results are also consistent with other reports [50].

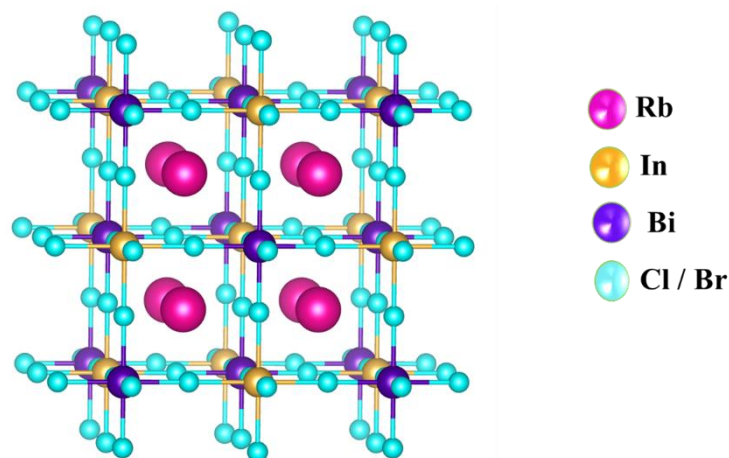


Figure 1. Generated cubic crystal structure of $\text{Rb}_2\text{InBiX}_6$ ($X = \text{Cl}, \text{Br}$) compounds.

Table 1. Computed lattice parameter a (Å), volume V , formation energy E_f , tolerance factor (τ), and bond-length (Å) for $\text{Rb}_2\text{InBiX}_6$ ($X = \text{Cl}, \text{Br}$) compounds using PBE-GGA approach.

Compound Name	a (Å)	V (a.u. ³)	E_f (eV/atom)	Tolerance Factor (τ)	Bond Length (Å)
$\text{Rb}_2\text{InBiCl}_6$	11.38	1474.04	−1.57	0.95	In-Cl = 2.97 Bi-Cl = 2.71
$\text{Rb}_2\text{InBiBr}_6$	11.87	1673.30	−1.37	0.93	In-Br = 3.05 Bi-Br = 2.88
$\text{Cs}_2\text{KTiCl}_6$ [50]	11.31			0.94	

We estimated the formation energy for material stability, and the results are shown in Table 2. Their mathematical expression are as follows.

$$E_f = E_{\text{Total}}^{\text{Rb}_2\text{InBiX}_6} - 2E_{\text{Rb}}^{\text{bulk}} - E_{\text{In}}^{\text{bulk}} - E_{\text{Bi}}^{\text{bulk}} - 6E_{\text{X}}^{\text{bulk}} \quad (1)$$

The negative value of formation energy suggests the stability of the investigated compounds [51]. The average bond length can be used to calculate the tolerance factor (τ) of the double perovskite compounds, and thus, the crystal structure of the material can be estimated. The tolerance factor is influenced by temperature and pressure. A tolerance factor (τ) in the range 0.95–1.04 agrees with analytically derived values, suggesting the cubic crystal structure of the compounds under study [52]. The tolerance factor is estimated to be nearly equal to 1 signifying the cubic crystal structure of $\text{Rb}_2\text{InBiX}_6$ ($X = \text{Cl}, \text{Br}$) compounds. We used phonon dispersion simulations to study the dynamical stability of $\text{Rb}_2\text{InBiX}_6$ ($X = \text{Cl}, \text{Br}$) compounds. The Vienna ab-initio Simulation Package (VASP) is used to calculate the phonon spectra using the finite displacement method. Along high symmetry directions (M-K- Γ -A-L) in the first Brillouin zone, the phonon dispersion was computed (Figure 2). The balanced and unbalanced phonon structures are determined via the real and imaginary frequencies in the phonon plot for positive and negative frequencies, respectively. The dynamical stability of the investigated $\text{Rb}_2\text{InBiX}_6$ ($X = \text{Cl}, \text{Br}$) compounds are evidenced from the absence of an imaginary frequency at Γ -point [53,54]. The obtained results are consistent with other reports. The investigated $\text{Rb}_2\text{InBiX}_6$ ($X = \text{Cl}, \text{Br}$) compounds exhibit 10 atoms that constitute a total of 3 acoustic modes and 27 optical modes [24].

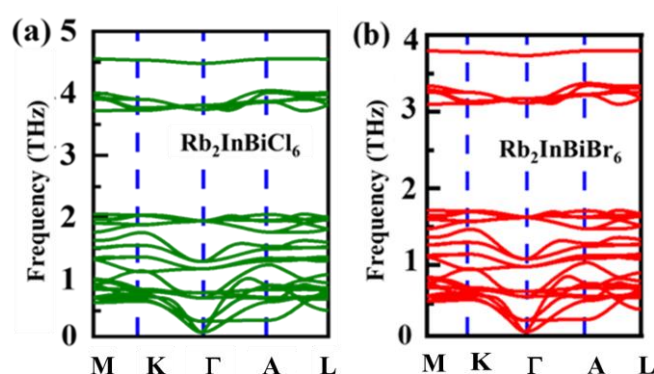


Figure 2. (a,b): Phonon dispersion plots for (a) $\text{Rb}_2\text{InBiCl}_6$ and (b) $\text{Rb}_2\text{InBiBr}_6$.

3.2. Mechanical Property

Designing solids for commercial manufacture for a variety of purposes requires consideration of mechanical qualities that includes second-order elastic constants (C_{ij}), bulk modulus (B), shear modulus (G), Pung ratio (B/G), anisotropy (A), etc. The strength of the dimensional structure in the cubic system is determined via three distinct elastic constants, C_{11} , C_{12} , and C_{44} . Where C_{11} represents the stiffness of materials against strains, C_{12} signifies shear stress, and C_{44} denotes opposition to shear deformation [55]. The computed

elastic constants for cubic double perovskite $\text{Rb}_2\text{InBiX}_6$ ($X = \text{Cl}, \text{Br}$) compounds are represented in Table 2. To confirm the stability of the compounds under examination, the Born-Huang stability criterion [56] is taken into account, which is:

$$(C_{11} - C_{12})/2 > 0, (C_{11} + 2C_{12}) > 0, C_{11} > 0 \quad (2)$$

Our calculations show that the compounds meet the Born-Huang stability criterion, indicating their stability. Other elastic constants for cubic structure such as bulk modulus (B), shear modulus (G), Young modulus (Y), Poisson's ratio (ν), and anisotropy (A) are computed using the below formulae.

$$B = \frac{C_{11} + 2C_{12}}{3} \quad (3)$$

$$G = \frac{C_{11} - C_{12}}{2} \quad (4)$$

$$Y = \frac{9GB}{3B + G} \quad (5)$$

$$\nu = \frac{3B - 2G}{2(3B + G)} \quad (6)$$

$$A = \frac{2C_{44}}{C_{11} - C_{12}} \quad (7)$$

The bulk modulus (B) of a material (when subjected to pressure) indicates how resistant the material is to volume change. While the shear modulus (G) represents the crystal's resistance to plastic deformation, the high B value signifies good crystal strength. The computed values of B are 18.08 GPa, 33.97 GPa for $\text{Rb}_2\text{InBiX}_6$ ($X = \text{Cl}, \text{Br}$) compounds. Because $\text{Rb}_2\text{InBiBr}_6$ has a higher B value than $\text{Rb}_2\text{InBiCl}_6$, it is more resistant to volume variation than $\text{Rb}_2\text{InBiCl}_6$. Furthermore, $\text{Rb}_2\text{InBiBr}_6$ has a greater G (9.30) than $\text{Rb}_2\text{InBiCl}_6$ (8.48). As a result, $\text{Rb}_2\text{InBiBr}_6$ has a significant resistance to transverse bending [57]. The brittleness or ductility of a material is determined via Pugh's ratio (B/G) [58]. The crystal is ductile if the B/G ratio is more than 1.75; otherwise, it is brittle [59]. The estimated B/G for $\text{Rb}_2\text{InBiX}_6$ ($X = \text{Cl}, \text{Br}$) compounds is shown in Table 2, indicating that the compounds under consideration are ductile. To identify between brittleness and ductility, Frantsevich et al. used Poisson's ratio (ν); 0.26 is the key value for both brittle and ductile properties. When the ν goes below 0.26, the compound is brittle; when it rises over 0.26, it becomes ductile. The calculated ν for the $\text{Rb}_2\text{InBiX}_6$ ($X = \text{Cl}, \text{Br}$) compounds is 0.29 and 0.37, indicating that the materials are ductile by nature. This is again confirmed from Cauchy pressure [60], which is computed as $C_p = C_{12} - C_{44}$, as listed in Table 2. Cauchy pressure values indicate that the compounds under investigation are ductile. The ionic (covalent) nature of the crystal bond can be determined using the positive (negative) value of the Cauchy pressure. The positive Cauchy pressures of the double perovskites $\text{Rb}_2\text{InBiX}_6$ ($X = \text{Cl}, \text{Br}$) compounds show that these are ionic in nature. $A = 1$ implies isotropic, while $1 < A < 1$ denotes anisotropic crystals [61,62]. The melting point T_m and Debye temperature (θ_D), two thermodynamic parameters related to elastic characteristics, were also investigated [63]. Using the following relation, the θ_D was calculated from the mean sound velocity (V_m):

$$\theta_D = \frac{h}{K_B} \left[\frac{3n}{4\pi} \left(\frac{N_A \rho}{M} \right) \right]^{-\frac{1}{3}} V_m \quad (8)$$

where k is Boltzmann's constant, h is Planck's constant, N_A is Avogadro's number, ρ is the density of the material, M is the molecular weight, and n is the number of atoms in a single

cell. The computed Debye temperature is given in Table 2. The mean sound speed of the investigated substances was calculated using [64]:

$$V_m = \left[\frac{1}{3} \left(\frac{2}{v_t^3} + \frac{1}{v_l^3} \right) \right]^{-\frac{1}{3}} \quad (9)$$

where the longitudinal and transverse components of sound velocity are v_l and v_t , calculated using the shear modulus and bulk modulus, respectively, as

$$v_t = \sqrt{\frac{G}{\rho}}, \quad v_l = \sqrt{\frac{3B + 4G}{3\rho}} \quad (10)$$

Table 2 provides the computed values of v_t , v_l , V_m , θ_D , and T_m .

Table 2. Computed values of elastic constants C_{11} , C_{12} , C_{44} in (GPa), bulk modulus B (GPa), shear modulus G (GPa), Young's modulus Y (GPa), Poisson's ratio ν , Zener anisotropy factor (A), B/G ratio, Cauchy pressure ($C_{12} - C_{44}$), and melting temperature T_m (K) for Rb_2InBiX_6 ($X = Cl, Br$) compounds using PBE-GGA approach.

Parameters	$Rb_2InBiCl_6$	$Rb_2InBiBr_6$	Cs_2LiYBr_6 [65]
C_{11}	44.32	61.81	45.73
C_{12}	4.97	20.05	11.88
C_{44}	1.02	1.58	10.54
B	18.08	33.97	23.16
G	8.48	9.30	12.75
Y	22.01	25.56	32.33
ν	0.29	0.37	0.26
B/G	2.13	3.65	1.81
$C_{12} - C_{44}$	3.95	18.47	1.33
A	0.05	0.07	
θ_D	126.6	119.1	
V_{tran}	1245	1203	
V_{long}	2759	3202	
$V_{avg.}$	1404	1365	
T_m	494.8	643.2	

3.3. Electronic Properties

The electronic characteristics of cubic Rb_2InBiX_6 ($X = Cl, Br$) compounds have been studied based on band structure density of states (DOS) and bonding nature has been addressed in terms of charge density distribution. The electronic band structure of the studied Rb_2InBiX_6 ($X = Cl, Br$) double perovskite compounds was computed along the high symmetry directions (M-K- Γ -A-L) in the Brillouin Zone and is presented in Figure 3a-j. The approximations, namely, PBE-LDA, PBE-GGA, PBE-sol, mBJ, and HSE, seem to have a similar band structure with a fermi level at 0. eV predicts the semiconductor nature of the compounds having a band gap of 1.15 eV, 1.27 eV, 1.50 eV, 1.61 eV, and 1.81 eV for $Rb_2InBiCl_6$ and 0.64 eV, 0.73 eV, 0.97 eV, 1.22 eV, and 1.32 eV for $Rb_2InBiBr_6$ compounds, respectively. A significant improvement is seen when compared to other experimental and theoretical studies when the modified Becke-Johnson (mBJ) exchange potential is employed to correct the underestimating band gap, as represented in Table 3. Furthermore, both materials have a direct band gap character due to having the same high symmetry K-points, as shown in Figure 3a-j [53].

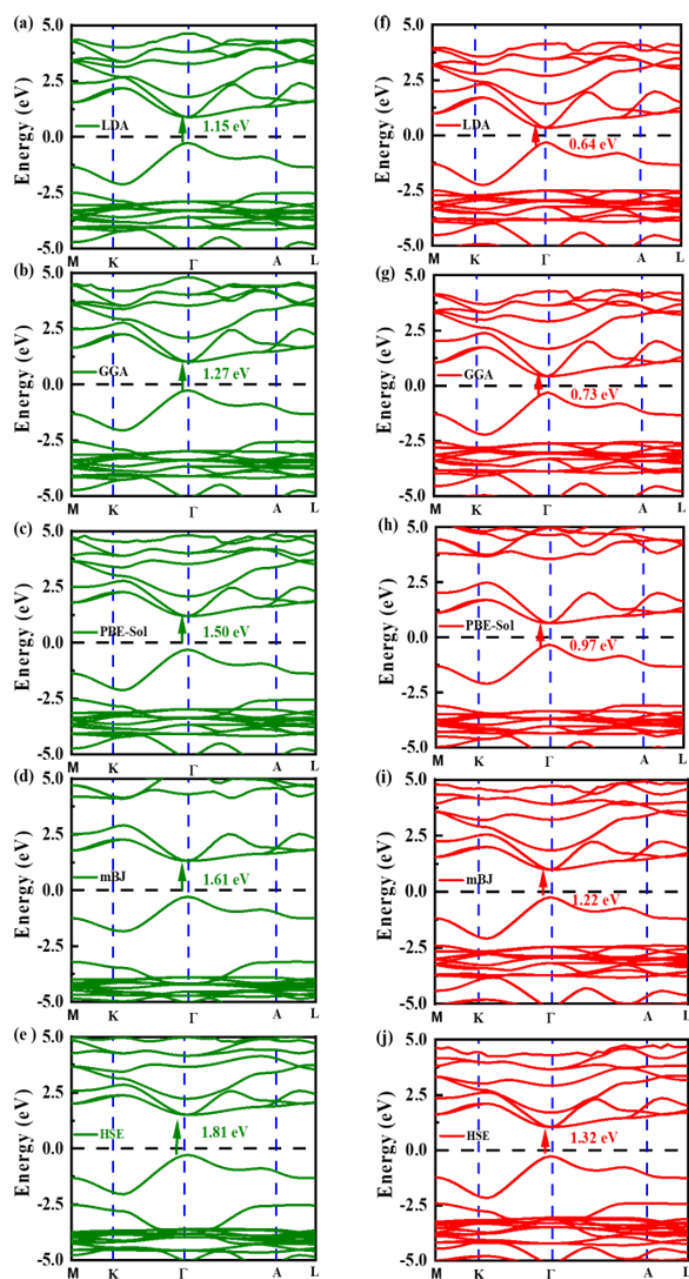


Figure 3. Band structure for (a–e) $\text{Rb}_2\text{InBiCl}_6$ and (f–j) $\text{Rb}_2\text{InBiBr}_6$ using different exchange correlation functionals.

The combined TDOS and PDOS of $\text{Rb}_2\text{InBiX}_6$ ($X = \text{Cl}, \text{Br}$) double perovskite compounds are shown in Figure 4a,b. Comprehensive information about elemental contribution is provided by the plot. The density of states contour shows that in the range 0 to 4 eV the bands formed due to Bi/In atoms, whereas a top of valence band in the range -4 to 0 eV is formed due to Cl/Br atoms with a minor contribution of Rb atoms for the investigated $\text{Rb}_2\text{InBiX}_6$ ($X = \text{Cl}, \text{Br}$) compounds. Bands between 2.5 and 4 eV are produced by the Bi atom in the conduction band. The hybridization of the Bi atom with a small contribution of Rb atoms results in the bands that are within the higher energy level of the conduction band.

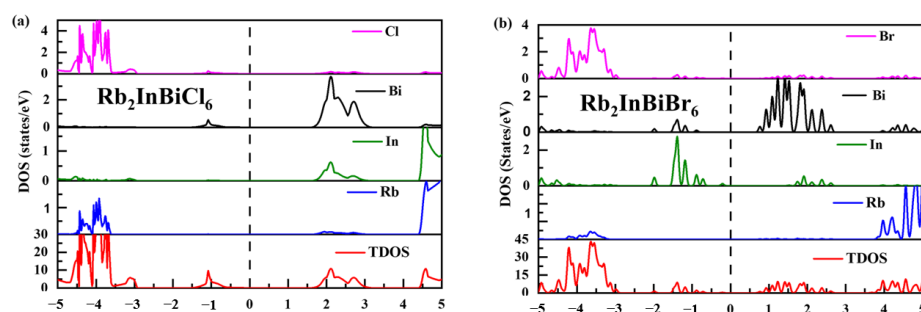


Figure 4. (a,b): Calculated electronic properties with (a,b) TDOS and PDOS for $\text{Rb}_2\text{InBiX}_6$ ($X = \text{Cl}, \text{Br}$) compounds using mBJ approach.

To better understand the photovoltaic characteristics which are significantly affected by resistivity, carrier mobility as well as the optical response of free carriers, study on the effective masses of carriers (holes and electrons) is essential [66]. The following formula is used to compute the effective mass of carriers in $\text{Rb}_2\text{InBiX}_6$ ($X = \text{Cl}, \text{Br}$) [67].

$$\frac{1}{m^*} = \frac{1}{\hbar^2} \frac{d^2 E_n(\mathbf{k})}{d\mathbf{k}^2} \quad (11)$$

For these perovskite materials, the computed effective mass values are given in Table 3. The findings show that the effective mass of carriers (electrons and holes) in the studied perovskite compounds are relatively low. For photovoltaic materials, the lower effective mass is very advantageous since it facilitates the transfer of carriers. This suggests that the double perovskite $\text{Rb}_2\text{InBiX}_6$ ($X = \text{Cl}, \text{Br}$) may prove to be efficient in photovoltaics.

Table 3. Computed band gap using different exchange correlation functional, effective mass of electron (m_e^*) and holes (m_h^*), Bader charges (using PBE-GGA approach) for $\text{Rb}_2\text{InBiX}_6$ ($X = \text{Cl}, \text{Br}$) compound.

Compound	LDA	GGA	PBE-Sol	mBJ	HSE	Effective Mass	Bader Charge
$\text{Rb}_2\text{InBiCl}_6$	1.15	1.27	1.50	1.61	1.81	$m_e^* = 0.76$ $m_h^* = 0.91$	Rb = 0.91 In = 0.89 Bi = 1.65 Cl = -0.72
$\text{Cs}_2\text{InAgCl}_6$ [68]				2.49			
$\text{Rb}_2\text{InBiBr}_6$	0.64	0.73	0.97	1.22	1.32	$m_e^* = 0.72$ $m_h^* = 0.80$	Rb = 0.88 In = 0.67 Bi = 1.34 Br = -0.63
$\text{Cs}_2\text{InAgBr}_6$ [68]				1.38			

3.4. ELF and Bader Charge

The bonding characteristics of the compounds can be obtained from charge density and its distribution plot [54,69]. Along the body diagonal plane, Figure 5a,b depicts the spatial charge configuration for the halogen-based double perovskite. The charge distributions of the Rb and In atoms are perfectly spherical, with no overlap between the charge contours of the Cl/Br atom. It was discovered that there was an ionic bond between the Rb and In and the Cl/Br atom. The charge distribution of the Bi, on the other hand, fluctuates from perfectly spherical to deformed, resulting in covalent bonding with the Cl/Br atom (dumb-bell type). This is again confirmed from the Bader charge analysis, whereby Br accepts electrons from the Bi-network, as given in Table 3.

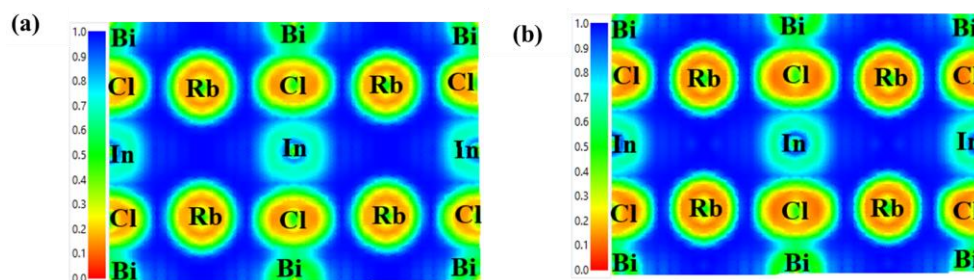


Figure 5. (a,b) Electron localization function (ELF) for $\text{Rb}_2\text{InBiX}_6$ ($X = \text{Cl}, \text{Br}$) compounds along (100) plane.

3.5. Optical Properties

The studied double perovskite compounds ($\text{Rb}_2\text{InBiX}_6$ ($X = \text{Cl}, \text{Br}$)) have the features of direct band gaps and wide band gaps, which sparked our interest in finding out more about their optical properties [70]. Analysing the material optical properties is essential to obtain the precise information required for usage in optoelectronic and photovoltaic application; to investigate energy-dependent optical properties, the dielectric functions are considered. The complex dielectric function $\varepsilon(\omega)$ consists of two parts, real and imaginary, which can be expressed as

$$\varepsilon = \varepsilon_1(\omega) + i\varepsilon_2(\omega) \quad (12)$$

The imaginary part, $\varepsilon_2(\omega)$ [71], is due to inter-band and intra-band transitions that display probable transitions along k -vectors from the occupied to unoccupied states over the Brillouin zone (BZ) and that are reliant on DOS and the momentum matrix P and can be mathematically defined as

$$\varepsilon_2(\omega) = \frac{e^2\hbar}{\pi m^2 \omega^2} \sum \int |M_{v,c}(\mathbf{k})|^2 \delta[\omega_{vc}(\mathbf{k}) - \omega] d^3k \quad (13)$$

where p stands for the moment matrix element in between the states of band α and β under the crystal momentum k , and c_k and v_k are the crystal wave functions relative to the CB and VB along crystal wave vector k . The $\varepsilon_1(\omega)$ from the imaginary dielectric can be computed as [72]

$$\varepsilon_1(\omega) = 1 + \frac{2}{\pi} P \int_0^\infty \frac{\omega' \varepsilon_2(\omega') d\omega'}{(\omega'^2 - \omega^2)} \quad (14)$$

The knowledge of both the real and imaginary parts of the dielectric function allow us to calculate other important optical functions such as the refractive index $n(\omega)$, the optical absorption coefficient $\alpha(\omega)$, etc.

Figure 6a,b illustrates the fluctuation of real $\varepsilon_1(\omega)$ and imaginary $\varepsilon_2(\omega)$ dielectric function with photon energy (0 eV to 8 eV) for $\text{Rb}_2\text{InBiX}_6$ ($X = \text{Cl}, \text{Br}$). The amount of polarisation that occurs when light interacts with a medium is quantified as $\varepsilon_1(\omega)$, and the amount of energy loss because of light dispersion is evaluated via $\varepsilon_2(\omega)$. At zero energy level the $\varepsilon_1(\omega)$ is termed as static dielectric constant $\varepsilon_1(0)$. The computed $\varepsilon_1(0)$ values are presented in Table 4. It is noticed that $\varepsilon_1(0)$ increases from Cl to Br due to the greater polarizability of larger halogens. Moreover, these values are inversely correlated with their relevant band gaps retrieved from the computed band structures, and accordingly, Penn's model (i.e., $\varepsilon_1(0) = 1 + (\hbar\omega_p/E_g)$) may be demonstrated to be satisfied [73]. From Figure 6a it is observed that $\varepsilon_1(\omega)$ increased with photon energy with multiple peaks that are known as relaxation peaks. Relaxation time or frequency can be determined from these peaks. Additionally, because of the inverse relationship between the relaxation frequency and the net mass of oscillating atoms, the relaxation peaks are shifted towards lower energy. As observed from Figure 6a, the main peaks of $\varepsilon_1(\omega)$ lie in the visible range for the investigated $\text{Rb}_2\text{InBiX}_6$ ($X = \text{Cl}, \text{Br}$) compounds. The refractive index $n(\omega)$ in the energy range is computed using $n(\omega) = \sqrt{\varepsilon_1(\omega)}$. As a result, $n(\omega)$ exhibits behaviour that is

similar to that of $\varepsilon_1(\omega)$, as shown in Figure 6c. The computed values of the highest $n(\omega)$ are represented in Table 4.

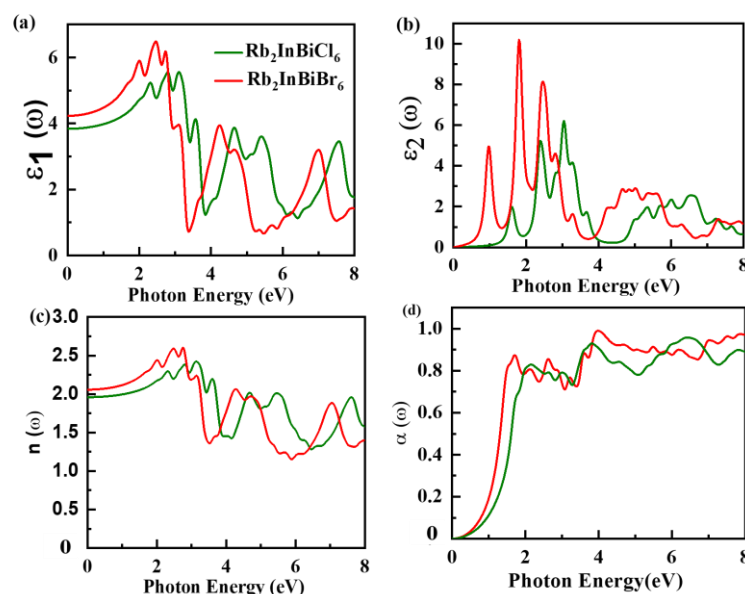


Figure 6. Computed (a) real part $\varepsilon_1(\omega)$, (b) imaginary part $\varepsilon_2(\omega)$ of dielectric, (c) refractive index $n(\omega)$, (d) absorption coefficient $\alpha(\omega)$ for Rb₂InBiX₆ (X = Cl, Br) compounds.

Table 4. Calculated optical and transport properties for double perovskite Rb₂InBiX₆ (X = Cl, Br) compounds using mBJ approach.

Material Property		Rb ₂ InBiCl ₆	Rb ₂ AlInCl ₆ [38]	Rb ₂ InBiBr ₆	Rb ₂ AlInBr ₆ [38]
Optical properties	$\varepsilon_1(0)$	3.81	4.52	4.24	5.51
	$n(0)$	1.94	2.12	2.05	2.34
	S (μ VK)	335	232.13	550	229.15
Transport properties (300 K)	σ/τ (Ω ms) ⁻¹ (10^{18})	0.01	0.03	0.07	0.046
	k/τ (W/mKs) (10^{15})	0.13	9.6	0.20	10.6
	PF (10^{10})	0.34	0.23	0.86	0.25
	(W/K ² ms)				

The variation of $\varepsilon_2(\omega)$ with photon energy is represented in Figure 6b. The imaginary component of the dielectric function depicts absorption qualities as well as the optical band gap [74]. Up to 1.08 eV and 0.51 eV, no absorption is seen that would suggest the optical band gap is approximately comparable to the electrical band gap. Figure 6d represents variation of absorption coefficient $\alpha(\omega)$ with photon energy. It exhibits the same pattern as $\varepsilon_2(\omega)$. The different peaks in the plot represent the energy loss due to the material absorption. The presence of absorption peaks in the visible spectrum indicates that the studied compounds exhibit good absorption performance in this region. The detailed analysis of optical properties shows outstanding photoelectric characteristics, indicating a great deal of potential for usage in the absorber layer of solar cells.

In semiconductors, photon absorption causes electrons in the VB to be elevated to the CB, creating free charge carriers, such as holes in the VB and electrons in the CB. The coulombic interaction photoexcited electrons and holes result in “excitonic effects”, which modify the optoelectronic behaviour of semiconductors. The Mott-Wannier model’s equation [75] was used to compute the exciton binding energies of Rb₂InBiX₆ (X = Cl, Br) compounds.

$$E_b^{\text{ex}} = \frac{e^4}{2(4\pi\varepsilon_0\hbar^2)^2} \frac{\mu_r}{\varepsilon_1(0)^2} \approx 13.56 \frac{\mu_r}{m_e} \frac{1}{\varepsilon_1(0)^2} \quad (15)$$

here $\mu_r = \frac{m_e^* \times m_h^*}{m_e^* + m_h^*}$ is the exciton effective mass, $\epsilon_1(0)$ corresponds to static dielectric constant, and m_e^* and m_h^* denotes effective mass of electrons and holes. For $\text{Rb}_2\text{InBiX}_6$ ($X = \text{Cl}, \text{Br}$) compounds, the estimated exciton binding energy is 380.02, 280.63 meV, which is observed to be quite close to other reports [37].

3.6. Thermoelectric Property

Thermoelectric (TE) energy conversion, which incorporates waste heat recovery, is widely regarded as a viable power production technique. To explore the transport behaviour of cubic $\text{Rb}_2\text{InBiX}_6$ ($X = \text{Cl}, \text{Br}$) compounds, the BoltzTrap code is employed along with the constant relaxation time approximation. In this study, the Seebeck coefficient, electrical and thermal conductivity properties, and their correlations to temperature are investigated to determine the thermoelectric response of the examined compounds.

The magnitude of the transport properties are influenced by band structure, charge carrier type, and effective mass [76]. The carriers that participate in the transport phenomena (holes and electrons) are principally determined by their band gap. It is noticed that the band gap increases with application of mBJ as compared to GGA. The tuning of the band gap is the important aspect for determination of the Seebeck coefficient. Insulators show a high Seebeck coefficient, while metals show the lowest Seebeck coefficient [77]. The thermoelectric voltage generated due to the temperature gradient across two ends of a material is measured via the Seebeck coefficient, which is directly dependent on charge carriers. To have the best thermoelectric performance, the Seebeck coefficient should be high. For p-type materials, S is positive, but for n-type materials, it is negative [78]. The variation of S with temperature is represented in Figure 7a suggesting p-type behaviour with positive magnitude of the Seebeck coefficient. The magnitude of S was found to be 335 $\mu\text{V}/\text{K}$, 550 $\mu\text{V}/\text{K}$ for the studied $\text{Rb}_2\text{InBiX}_6$ ($X = \text{Cl}, \text{Br}$) compounds at room temperature, as shown in Table 4. Correspondingly, at a high temperature of 800 K the S was found to be 237 $\mu\text{V}/\text{K}$, 295 $\mu\text{V}/\text{K}$ for $\text{Rb}_2\text{InBiX}_6$ ($X = \text{Cl}, \text{Br}$) compounds, respectively. The ionic size increases from Cl to Br, which leads to loosely bound valence electrons that only need a very little amount of energy to break the bond. As a result, little excitation energy is needed due to band gap decreases from Cl to Br and the creation of free charge carriers rises, resulting in an increase in electrical conductivity. Similarly, as an atom changes from Cl to Br, S decreases because the potentials maintained across the sample edges may deteriorate as the band gap decreases and free charge carriers rise at lower exciting energies. Other reports on similar compounds support this; for instance, for S it is reported to be 250 $\mu\text{V}/\text{K}$, 246 $\mu\text{V}/\text{K}$ for $\text{Cs}_2\text{InBiX}_6$ ($X = \text{Cl}, \text{Br}$) [24], 232.13 $\mu\text{V}/\text{K}$, 229.15 $\mu\text{V}/\text{K}$ for $\text{Rb}_2\text{AlInX}_6$ ($X = \text{Cl}, \text{Br}$) [38], and 208 $\mu\text{V}/\text{K}$, 205 $\mu\text{V}/\text{K}$ for $\text{Cs}_2\text{InAgX}_6$ ($X = \text{Cl}, \text{Br}$) [68]. According to Figure 7b, the Seebeck coefficient is inversely associated to electrical conductivity and directly linked to the band gap. Furthermore, an ideal TE material has a Seebeck coefficient of more than 200 $\mu\text{V}/\text{K}$ suggesting a good thermoelectric response of the investigated compounds. Figure 7b shows the predicted electrical conductivity (σ/τ) with temperature variation. At room temperature, it is calculated to be $0.01 \times 10^{18} (\Omega\text{mS})^{-1}$, $0.07 \times 10^{18} (\Omega\text{mS})^{-1}$ for $\text{Rb}_2\text{InBiX}_6$ ($X = \text{Cl}, \text{Br}$) compounds. A comparative study of electrical conductivity at room temperature can be found in Table 4. The obtained σ/τ is comparable to other reports such as $0.01 \times 10^{18} (\Omega\text{mS})^{-1}$, $0.07 \times 10^{18} (\Omega\text{mS})^{-1}$ for $\text{Cs}_2\text{AgCrX}_6$ ($X = \text{Cl}, \text{Br}$) [37], $0.96 \times 10^{18} (\Omega\text{mS})^{-1}$ and $1.06 \times 10^{18} (\Omega\text{mS})^{-1}$ for $\text{Rb}_2\text{AlInX}_6$ ($X = \text{Cl}, \text{Br}$) compounds [38]. As the temperature rises, σ/τ increases as well, which is a common pattern for semiconductor materials [79]. At 800 K the σ/τ for $\text{Rb}_2\text{InBiX}_6$ ($X = \text{Cl}, \text{Br}$) are found to be $0.26 \times 10^{18} (\Omega\text{mS})^{-1}$, $0.46 \times 10^{18} (\Omega\text{mS})^{-1}$ respectively. The electrical conductivity of $\text{Rb}_2\text{InBiBr}_6$ is noticed to be high, which is due to the presence of high density of charge carriers, which enhances the electrical conductivity. Thermal lattice conductivity (κ/τ) is the result of the contributions of both electronic as well as lattice thermal conductivities. The electron and hole motion are responsible for electronic thermal conductivity, whereas lattice vibrations (phonons) are responsible for lattice thermal conductivity. Here, we have considered the electronic thermal conductivity (κ_e/τ) as it is only significant in the

electronic limit, as shown in Figure 7c [80]. It is observed that κ_e/τ increases significantly with temperature. The magnitude of κ_e/τ at ambient temperature (300 K) with comparison to reported compounds is presented in Table 4. Widemann Franz law (σ/κ) provides the relationship between electrical conductivity to thermal conductivity. The σ/κ was noticed to be in the order of 10^{-5} , signalling excellent electrical conductivity and reduced thermal conductivity [81]. The effectiveness of a thermoelectric compound can be determined from the power factor (PF), which is a product of the square of the Seebeck coefficient and electrical conductivity [82]. Figure 7d shows the calculated PF for the investigated $\text{Rb}_2\text{InBiX}_6$ ($X = \text{Cl}, \text{Br}$) compounds. The computed PF at 800 K is found to be $2.7 \times 10^{10} \text{ W/K}^2\text{ms}$, $3.1 \times 10^{10} \text{ W/K}^2\text{ms}$ for $\text{Rb}_2\text{InBiX}_6$ ($X = \text{Cl}, \text{Br}$) compounds. The high power factor at high temperatures shows that the compounds are suitable for usage in thermoelectric devices.

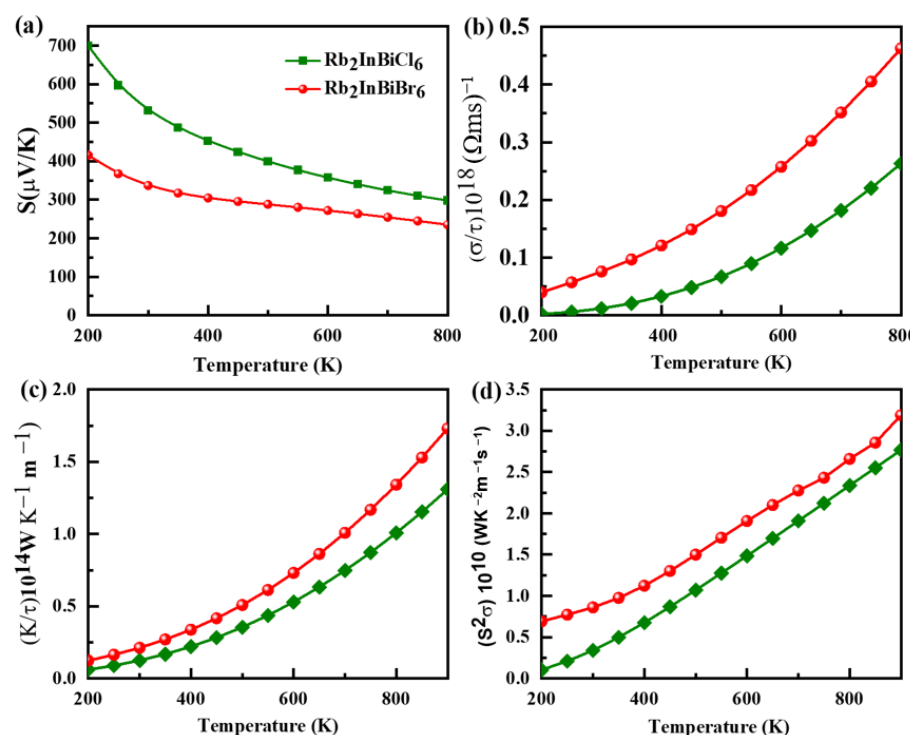


Figure 7. Computed values of (a) Seebeck coefficient (s), (b) electrical conductivity (σ/τ), (c) thermal conductivity (κ/τ), (d) power factor ($S^2\sigma$) with temperature.

4. Conclusions

In this study, density functional theory has been employed to analyse the physical properties of double perovskite $\text{Rb}_2\text{InBiX}_6$ ($X = \text{Cl}, \text{Br}$) compounds. According to the computed results, the investigated compounds are thermodynamically and mechanically stable, as evidenced from the formation energy, tolerance factor, and Born-Huang stability criterion. The Pung ratio value and Poisson ratio suggest that both $\text{Rb}_2\text{InBiX}_6$ ($X = \text{Cl}, \text{Br}$) compounds are ductile in nature. According to the band structure computed band gap using mBJ, the HSE are 1.61 eV, 1.81 eV for $\text{Rb}_2\text{InBiCl}_6$ and 1.22 eV, 1.32 eV for $\text{Rb}_2\text{InBiBr}_6$ compounds, respectively. The studied compounds have a significantly lower effective mass of electrons than other perovskite compounds, suggesting that they may have higher carrier mobility. Furthermore, the optical parameters of $\text{Rb}_2\text{InBiX}_6$ ($X = \text{Cl}, \text{Br}$) have been thoroughly examined in order to comprehend their optical features. The computed outcomes show that the compounds have outstanding light absorption and good dielectric characteristics. In the transport properties, we determined the power factor employing BoltzTraP software. The computed PF values at 800 K are $2.7 \times 10^{10} \text{ W/K}^2\text{ms}$, $3.1 \times 10^{10} \text{ W/K}^2\text{ms}$ for $\text{Rb}_2\text{InBiX}_6$ ($X = \text{Cl}, \text{Br}$) compounds. The potential application of $\text{Rb}_2\text{InBiX}_6$ ($X = \text{Cl}, \text{Br}$) compounds for the application of optoelectronic and thermoelectric devices is demonstrated via the

appropriate values of estimated parameters such as adequate direct band gap, excellent absorption spectra, and high power factor.

Author Contributions: Methodology, D.B.; software, S.K.M.; investigation, D.B.; resources, S.K.M.; writing—original draft preparation, D.B.; writing—review and editing, S.K.M.; visualization, S.K.M.; supervision, S.K.M. All authors have read and agreed to the published version of the manuscript.

Funding: This research received no external funding.

Data Availability Statement: The raw/processed data can be shared with reasonable request to the corresponding author.

Acknowledgments: One of the authors (Debidatta Behera) is thankful to Birla Institute of Technology, Ranchi, for the award of an institute fellowship.

Conflicts of Interest: The authors declare that they have no known competing financial interest or personal relationships that could have appeared to influence the work reported in this paper.

References

1. Elsheikh, M.H.; Shnawah, D.A.; Sabri, M.F.M.; Said, S.B.M.; Hassan, M.H.; Bashir, M.B.A.; Mohamad, M. A review on thermoelectric renewable energy: Principle parameters that affect their performance. *Renew. Sustain. Energy Rev.* **2014**, *30*, 337–355. [[CrossRef](#)]
2. Zheng, X.F.; Liu, C.X.; Yan, Y.Y.; Wang, Q. A review of thermoelectrics research—Recent developments and potentials for sustainable and renewable energy applications. *Renew. Sustain. Energy Rev.* **2014**, *32*, 486–503. [[CrossRef](#)]
3. Goldsmid, H.J.; Goldsmid, H.J. *The Seebeck and Peltier Effects*; Morgan & Claypool Publishers: New York, NY, USA, 2017.
4. Steele, W.H. A new thermoelectric phenomenon. *Science* **1893**, *562*, 256. [[CrossRef](#)] [[PubMed](#)]
5. Champier, D. Thermoelectric generators: A review of applications. *Energy Convers. Manag.* **2017**, *140*, 167–181. [[CrossRef](#)]
6. Mingo, N. Thermoelectric figure of merit and maximum power factor in III–V semiconductor nanowires. *Appl. Phys. Lett.* **2004**, *84*, 2652–2654. [[CrossRef](#)]
7. Nemir, D.C.; Beck, J. On the Significance of the Thermoelectric Figure of Merit *Z. J. Electron. Mater.* **2010**, *39*, 1897–1901. [[CrossRef](#)]
8. Zhao, L.-D.; Lo, S.-H.; Zhang, Y.; Sun, H.; Tan, G.; Uher, C.; Wolverton, C.; Dravid, V.P.; Kanatzidis, M.G. Ultralow thermal conductivity and high thermoelectric figure of merit in SnSe crystals. *Nature* **2014**, *508*, 373–377. [[CrossRef](#)]
9. Aswal, D.K.; Basu, R.; Singh, A. Key issues in development of thermoelectric power generators: High figure-of-merit materials and their highly conducting interfaces with metallic interconnects. *Energy Convers. Manag.* **2016**, *114*, 50–67. [[CrossRef](#)]
10. Dahbi, S.; Tahiri, N.; El Bounagui, O.; Ez-Zahraoui, H. Electronic, optical, and thermoelectric properties of perovskite BaTiO₃ compound under the effect of compressive strain. *Chem. Phys.* **2021**, *544*, 111105. [[CrossRef](#)]
11. Maiti, T.; Saxena, M.; Roy, P. Double perovskite (Sr₂B' B "O₆) oxides for high-temperature thermoelectric power generation—A review. *J. Mater. Res.* **2019**, *34*, 107–125. [[CrossRef](#)]
12. Arribi, P.V.; García-Fernández, P.; Junquera, J.; Pardo, V. Efficient thermoelectric materials using nonmagnetic double perovskites with d⁰/d⁶ band filling. *Phys. Rev.* **2016**, *94*, 35124. [[CrossRef](#)]
13. Ricciarelli, D.; Kaiser, W.; Mosconi, E.; Wiktor, J.; Ashraf, M.W.; Malavasi, L.; Ambrosio, F.; De Angelis, F. Reaction Mechanism of Photocatalytic Hydrogen Production at Water/Tin Halide Perovskite Interfaces. *ACS Energy Lett.* **2022**, *7*, 1308–1315. [[CrossRef](#)]
14. Irfan, R.M.; Tahir, M.H.; Iqbal, S.; Nadeem, M.; Bashir, T.; Maqsood, M.; Zhao, J.; Gao, L. Co₃C as a promising cocatalyst for superior photocatalytic H₂ production based on swift electron transfer processes. *J. Mater. Chem.* **2021**, *9*, 3145–3154. [[CrossRef](#)]
15. Bhamu, K.C.; Soni, A.; Sahariya, J. Revealing optoelectronic and transport properties of potential perovskites Cs₂PdX₆ (X = Cl, Br): A probe from density functional theory (DFT). *Sol. Energy* **2018**, *162*, 336–343. [[CrossRef](#)]
16. Usman, M.; Yan, Q. Recent Advancements in Crystalline Pb-Free Halide Double Perovskites. *Crystals* **2020**, *10*, 62. [[CrossRef](#)]
17. Yan, L.; Zhao, L.; Zhao, C.; Lin, S. Theoretical Understanding of Thermoelectric Energy Conversion Efficiency in Lead-Free Halide Double Perovskites Showing Intrinsic Defect Tolerance. *Appl. Therm. Eng.* **2022**, *215*, 119024. [[CrossRef](#)]
18. Zhao, X.-G.; Yang, J.-H.; Fu, Y.; Yang, D.; Xu, Q.; Yu, L.; Wei, S.-H.; Zhang, L. Design of Lead-Free Inorganic Halide Perovskites for Solar Cells via Cation-Transmutation. *J. Am. Chem. Soc.* **2017**, *139*, 2630–2638. [[CrossRef](#)]
19. Ghosh, S.; Shankar, H.; Kar, P. Recent developments of lead-free halide double perovskites: A new superstar in the optoelectronic field. *Mater. Adv.* **2022**, *3*, 3742–3765. [[CrossRef](#)]
20. Ravi, V.K.; Singhal, N.; Nag, A. Initiation and future prospects of colloidal metal halide double-perovskite nanocrystals: Cs₂AgBiX₆ (X = Cl, Br, I). *J. Mater. Chem.* **2018**, *6*, 21666–21675. [[CrossRef](#)]
21. Haque, E.; Hossain, M.A. Origin of ultra-low lattice thermal conductivity in Cs₂BiAgX₆ (X = Cl, Br) and its impact on thermoelectric performance. *J. Alloys Compd.* **2018**, *748*, 63–72. [[CrossRef](#)]
22. Murtaza, G.; Alshahrani, T.; Khalil, R.A.; Mahmood, Q.; Flemman, T.H.; Althib, H.; Laref, A. Lead Free Double Perovskites Halides X₂AgTiCl₆ (X = Rb, Cs) for solar cells and renewable energy applications. *J. Solid State Chem.* **2021**, *297*, 121988. [[CrossRef](#)]

23. Noor, N.; Iqbal, M.W.; Zelai, T.; Mahmood, A.; Shaikh, H.; Ramay, S.M.; Al-Masry, W. Analysis of Direct Band Gap A₂ScInI₆ (A = Rb, Cs) Double Perovskite Halides Using DFT Approach for Renewable Energy Devices. *J. Mater. Res. Technol.* **2021**, *13*, 2491–2500. [[CrossRef](#)]
24. Aslam, F.; Ullah, H.; Hassan, M. Theoretical investigation of Cs₂InBiX₆ (X = Cl, Br, I) double perovskite halides using first-principle calculations. *Mater. Sci. Eng.* **2021**, *274*, 115456. [[CrossRef](#)]
25. Zhou, X.; Jankowska, J.; Dong, H.; Prezhdo, O.V. Recent theoretical progress in the development of perovskite photovoltaic materials. *J. Energy Chem.* **2018**, *27*, 637–649. [[CrossRef](#)]
26. Shi, W.; Cai, T.; Wang, Z.; Chen, O. The effects of monovalent metal cations on the crystal and electronic structures of Cs₂MBiCl₆ (M = Ag, Cu, Na, K, Rb, and Cs) perovskites. *J. Chem. Phys.* **2020**, *153*, 141101. [[CrossRef](#)]
27. Romani, L.; Speltini, A.; Dibenedetto, C.N.; Listorti, A.; Ambrosio, F.; Mosconi, E.; Simbula, A.; Saba, M.; Profumo, A.; Quadrelli, P. Experimental Strategy and Mechanistic View to Boost the Photocatalytic Activity of Cs₃Bi₂Br₉ Lead-Free Perovskite Derivative by g-C₃N₄ Composite Engineering. *Adv. Funct. Mater.* **2021**, *31*, 2104428. [[CrossRef](#)]
28. Shafi, Z.; Ahmad, Z.; Joya, K.S.; Iqbal, S.; Khan, M.N. Designing of noble metal free high performance mesoporous electrocatalysts for water splitting. *Int. J. Hydrogen Energy* **2021**, *46*, 39799–39809. [[CrossRef](#)]
29. Bibi, A.; Lee, I.; Nah, Y.; Allam, O.; Kim, H.; Quan, N.L.; Tang, J.; Walsh, A.; Jang, S.S.; Sargent, E.H. Lead-free halide double perovskites: Toward stable and sustainable optoelectronic devices. *Mater. Today* **2021**, *49*, 123–144. [[CrossRef](#)]
30. Savory, C.N.; Walsh, A.; Scanlon, D.O. Can Pb-Free Halide Double Perovskites Support High-Efficiency Solar Cells? *ACS Energy Lett.* **2016**, *1*, 949. [[CrossRef](#)]
31. Xiao, Z.; Meng, W.; Wang, J.; Yan, Y. Thermodynamic stability and defect chemistry of bismuth-based lead-free double perovskites. *ChemSusChem* **2016**, *9*, 2628–2633. [[CrossRef](#)]
32. Filip, M.R.; Hillman, S.; Haghghirad, A.A.; Snaith, H.J.; Giustino, F. Band gaps of the lead-free halide double perovskites Cs₂BiAgCl₆ and Cs₂BiAgBr₆ from theory and experiment. *J. Phys. Chem. Lett.* **2016**, *7*, 2579–2585. [[CrossRef](#)]
33. Wei, F.; Deng, Z.; Sun, S.; Hartono, N.T.P.; Seng, H.L.; Buonassisi, T.; Bristowe, P.D.; Cheetham, A.K. Enhanced visible light absorption for lead-free double perovskite Cs₂AgSbBr₆. *Chem. Commun.* **2019**, *55*, 3721–3724. [[CrossRef](#)] [[PubMed](#)]
34. Luo, J.; Li, S.; Wu, H.; Zhou, Y.; Li, Y.; Liu, J.; Li, J.; Li, K.; Yi, F.; Niu, G. Cs₂AgInCl₆ double perovskite single crystals: Parity forbidden transitions and their application for sensitive and fast UV photodetectors. *ACS Photon.* **2018**, *5*, 398–405. [[CrossRef](#)]
35. Haque, E.; Hossain, M.A. High Seebeck coefficient and ultra-low lattice thermal conductivity in Cs₂InAgCl₆. *arXiv* **2018**, arXiv:1802.08136.
36. Mukhtar, M.W.; Ramzan, M.; Rashid, M.; Hussain, A.; Naz, G.; Ciftci, Y.O.; Dahshan, A.; Znaidia, S. Systematic study of optoelectronic and thermoelectric properties of new lead-free halide double perovskites A₂KGaI₆ (A = Cs, Rb) for solar cell applications via ab-initio calculations. *Mater. Sci. Eng.* **2022**, *285*, 115957. [[CrossRef](#)]
37. Saeed, M.; Haq, I.U.; Saleemi, A.S.; Rehman, S.U.; Haq, B.U.; Chaudhry, A.R.; Khan, I. First-principles prediction of the ground-state crystal structure of double-perovskite halides Cs₂AgCrX₆ (X = Cl, Br, and I). *J. Phys. Chem. Solids* **2022**, *160*, 110302. [[CrossRef](#)]
38. Iqbal, S.; Mustafa, G.M.; Asghar, M.; Noor, N.A.; Iqbal, M.W.; Mahmood, A.; Shin, Y.-H. Tuning the optoelectronic and thermoelectric characteristics of narrow bandgap Rb₂AlInX₆ (X = Cl, Br, I) double perovskites: A DFT study. *Mater. Sci. Semicond. Process.* **2022**, *143*, 106551. [[CrossRef](#)]
39. Harikesh, P.C.; Mulmudi, H.K.; Ghosh, B.; Goh, T.W.; Teng, Y.; Thirumal, K.; Lockrey, M.; Weber, K.; Koh, T.M.; Li, S. Rb as an Alternative Cation for Templating Inorganic Lead-Free Perovskites for Solution Processed Photovoltaics. *Chem. Mater.* **2016**, *28*, 7496–7504. [[CrossRef](#)]
40. Saliba, M.; Matsui, T.; Domanski, K.; Seo, J.-Y.; Ummadisingu, A.; Zakeeruddin, S.M.; Correa-Baena, J.-P.; Tress, W.R.; Abate, A.; Hagfeldt, A. Incorporation of rubidium cations into perovskite solar cells improves photovoltaic performance. *Science* **2016**, *354*, 206–209. [[CrossRef](#)]
41. Blaha, P.; Schwarz, K.; Madsen, G.K.H.; Kvasnicka, D.; Luitz, J.; Laskowski, R.; Tran, F.; Marks, L.D. Wien2k. In *An Augmented Plane Wave+ Local Orbitals Program for Calculating Crystal Properties*; Schwarz, S., Ed.; Vienna University of Technology: Vienna, Austria, 2001.
42. Hohenberg, P.; Kohn, W. Density functional theory (DFT). *Phys. Rev.* **1964**, *136*, B864. [[CrossRef](#)]
43. Koller, D.; Tran, F.; Blaha, P. Improving the modified Becke-Johnson exchange potential. *Phys. Rev.* **2012**, *85*, 155109. [[CrossRef](#)]
44. Blaha, P.; Schwarz, K.; Sorantin, P.; Trickey, S. Full-potential, linearized augmented plane wave programs for crystalline systems. *Comput. Phys. Commun.* **1990**, *59*, 399–415. [[CrossRef](#)]
45. Jamal, M.; Bilal, M.; Ahmad, I.; Jalali-Asadabadi, S. IRelast package. *J. Alloys Compd.* **2018**, *735*, 569–579. [[CrossRef](#)]
46. Hafner, J. Ab-initio simulations of materials using VASP: Density-functional theory and beyond. *J. Comput. Chem.* **2008**, *29*, 2044–2078. [[CrossRef](#)]
47. Madsen, G.K.; Singh, D.J. BoltzTraP. A code for calculating band-structure dependent quantities. *Comput. Phys. Commun.* **2006**, *175*, 67–71. [[CrossRef](#)]
48. Anderson, M.; Greenwood, K.; Taylor, G.; Poepelmeier, K. B-cation arrangements in double perovskites. *Prog. Solid State Chem.* **1993**, *22*, 197–233. [[CrossRef](#)]
49. Haque, E.; Hossain, M.A. Electronic, phonon transport and thermoelectric properties of Cs₂InAgCl₆ from first-principles study. *Comput. Condens. Matter* **2019**, *19*, e00374. [[CrossRef](#)]

50. Albalawi, H.; Mustafa, G.M.; Saba, S.; Kattan, N.A.; Mahmood, Q.; Somaily, H.H.; Morsi, M.; Alharthi, S.; Amin, M.A. Study of Optical and Thermoelectric Properties of Double Perovskites Cs₂KTlX₆ (X = Cl, Br, I) for Solar Cell and Energy Harvesting. *Mater. Today Commun.* **2022**, *32*, 104083. [[CrossRef](#)]
51. Mahmood, Q.; Ghrib, T.; Rached, A.; Laref, A.; Kamran, M. Probing of mechanical, optical and thermoelectric characteristics of double perovskites Cs₂GeCl/Br₆ by DFT method. *Mater. Sci. Semicond. Process.* **2020**, *112*, 105009. [[CrossRef](#)]
52. Fedorovskiy, A.E.; Drigo, N.A.; Nazeeruddin, M.K. The role of Goldschmidt's tolerance factor in the formation of A₂BX₆ double halide perovskites and its optimal range. *Small Methods* **2020**, *4*, 1900426. [[CrossRef](#)]
53. Varadwaj, P.R. A₂AgCrCl₆ (A = Li, Na, K, Rb, Cs) halide double perovskites: A transition metal-based semiconducting material series with appreciable optical characteristics. *Phys. Chem. Chem. Phys.* **2020**, *22*, 24337–24350. [[CrossRef](#)]
54. Behera, D.; Sharma, R.; Ullah, H.; Waheed, H.S.; Mukherjee, S.K. Electronic, optical, and thermoelectric investigations of Zintl phase AAg₂Se₂ (A = Sr, Ba) compounds: A first first-principles approach. *J. Solid State Chem.* **2022**, *312*, 123259. [[CrossRef](#)]
55. Mouhat, F.; Coudert, F.-X. Necessary and sufficient elastic stability conditions in various crystal systems. *Phys. Rev.* **2014**, *90*, 224104. [[CrossRef](#)]
56. Waller, I. Dynamical theory of crystal lattices by M. Born and K. Huang. *Acta Crystallogr.* **1956**, *9*, 837–838. [[CrossRef](#)]
57. Choudary, M.Z.; Aldaghfag, S.A.; Yaseen, M.; Nazar, M.; Neffati, R. Study of elastic, structural, thermoelectric and optoelectronic characteristics of Na₂YCuX₆ (X = Br, Cl) halide double perovskites. *Phys. Scr.* **2022**, *97*, 105705.
58. Pugh, S.F. XCII. Relations between the elastic moduli and the plastic properties of polycrystalline pure metals. *Lond. Edinb. Dublin Philos. Mag. J. Sci.* **1954**, *45*, 823–843. [[CrossRef](#)]
59. Pugh, S.F.; Pugh, S.F.; Philo, M. The London, Edinburgh, and Dublin Philosophical Magazine and Journal of Science. *Taylor Fr.* **1954**, *45*, 823–843.
60. Eberhart, M.E.; Jones, T.E. Cauchy pressure and the generalized bonding model for nonmagnetic bcc transition metals. *Phys. Rev.* **2012**, *86*, 134106. [[CrossRef](#)]
61. Hossain, K.M.; Hasan, M.Z.; Ali, M.L. Narrowing bandgap and enhanced mechanical and optoelectronic properties of perovskite halides: Effects of metal doping. *AIP Adv.* **2021**, *11*, 15052. [[CrossRef](#)]
62. Zener, C. *Elasticity and Anelasticity of Metals*; University of Chicago Press: Chicago, IL, USA, 1948.
63. Anderson, O.L. A simplified method for calculating the debye temperature from elastic constants. *J. Phys. Chem. Solids* **1963**, *24*, 909–917. [[CrossRef](#)]
64. Schreiber, E.; Anderson, O.L.; Soga, N.; Bell, J.F. Elastic Constants and Their Measurement. *J. Appl. Mech.* **1975**, *42*, 747–748. [[CrossRef](#)]
65. Al-Qaisi, S.; Rai, D.P.; Haq, B.U.; Ahmed, R.; Vu, T.V.; Khuili, M.; Tahir, S.A.; Alhashim, H.H. First-principles investigation of structural, elastic, thermodynamic, electronic and optical properties of lead-free double perovskites halides: Cs₂LiYX₆ (X = Br, I). *Mater. Chem. Phys.* **2021**, *258*, 123945. [[CrossRef](#)]
66. Tang, Y.; Zhang, J.; Zhong, X.; Wang, Q.; Zhang, H.; Ren, C.; Wang, J. Revealing the structural, electronic and optical properties of lead-free perovskite derivatives of Rb₂SnX₆ (X = Cl, Br and I): A theory calculation. *Sol. Energy* **2019**, *190*, 272–277. [[CrossRef](#)]
67. Cohen, M.; Ham, F. Electron effective mass in solids—A generalization of Bardeen's formula. *J. Phys. Chem. Solids* **1960**, *16*, 177–183. [[CrossRef](#)]
68. Aslam, F.; Sabir, B.; Hassan, M. Structural, electronic, optical, thermoelectric, and transport properties of indium-based double perovskite halides Cs₂InAgX₆ (X = Cl, Br, I) for energy applications. *Appl. Phys.* **2021**, *127*, 1–12. [[CrossRef](#)]
69. Abraham, J.A.; Behera, D.; Kumari, K.; Srivastava, A.; Sharma, R.; Mukherjee, S.K. A comprehensive DFT analysis on structural, electronic, optical, thermoelectric, SLME properties of new Double Perovskite Oxide Pb₂ScBiO₆. *Chem. Phys. Lett.* **2022**, *806*, 139987. [[CrossRef](#)]
70. Wu, S.; Chen, Z.; Yip, H.-L.; Jen, A.K.-Y. The evolution and future of metal halide perovskite-based optoelectronic devices. *Matter* **2021**, *4*, 3814–3834. [[CrossRef](#)]
71. Gajdoš, M.; Hummer, K.; Kresse, G.; Furthmüller, J.; Bechstedt, F. Linear optical properties in the projector-augmented wave methodology. *Phys. Rev.* **2006**, *73*, 045112. [[CrossRef](#)]
72. Kuzmenko, A.B. Kramers–Kronig constrained variational analysis of optical spectra. *Rev. Sci. Instrum.* **2005**, *76*, 083108. [[CrossRef](#)]
73. Penn, D.R. Wave-Number-Dependent Dielectric Function of Semiconductors. *Phys. Rev.* **1962**, *128*, 2093–2097. [[CrossRef](#)]
74. Behera, D.; Manzoor, M.; Iqbal, M.W.; Lakra, S.; Mukherjee, S.K. Revealing Excellent Electronic, Optical, and Thermoelectric Behavior of EU Based Euag₂y₂ (Y = S/Se): For Solar Cell Applications. *Comput. Condens. Matter.* **2022**, *32*, e00723. [[CrossRef](#)]
75. Jong, U.-G.; Yu, C.-J.; Kim, Y.-S.; Kye, Y.-H.; Kim, C.-H. First-principles study on the material properties of the inorganic perovskite Rb_{1-x} Cs_xPbI₃ for solar cell applications. *Phys. Rev.* **2018**, *98*, 125116. [[CrossRef](#)]
76. Yaseen, M.; Butt, M.K.; Ashfaq, A.; Iqbal, J.; Almoneef, M.M.; Misbah, Iqbal, M.; Murtaza, A.; Larefa, A. Phase transition and thermoelectric properties of cubic KNbO₃ under pressure: DFT approach. *J. Mater. Res. Technol.* **2021**, *11*, 2106–2113. [[CrossRef](#)]
77. Zhang, X.; Zhao, L.-D. Thermoelectric materials: Energy conversion between heat and electricity. *J. Mater.* **2015**, *1*, 92–105. [[CrossRef](#)]
78. Wu, G.; Yu, X. Contributions of chemical potential to the diffusive Seebeck coefficient for bulk semiconductor materials. *Eur. Phys. J. Plus* **2020**, *135*, 1–15. [[CrossRef](#)]
79. Sajjad, M.; Mahmood, Q.; Singh, N.; Larsson, J.A. Ultralow Lattice Thermal Conductivity in Double Perovskite Cs₂PtI₆: A Promising Thermoelectric Material. *ACS Appl. Energy Mater.* **2020**, *3*, 11293–11299. [[CrossRef](#)]

80. Yaseen, M.S.; Murtaza, G.; Khalil, R.M.A. First principle study of structural, electronic, optical, and transport properties of ternary compounds NaGaX_2 ($X = \text{S, Se, and Te}$) in tetragonal chalcopyrite phase. *Opt. Quantum Electron.* **2019**, *51*, 1–14. [[CrossRef](#)]
81. Stojanovic, N.; Maithripala, D.H.S.; Berg, J.M.; Holtz, M. Thermal conductivity in metallic nanostructures at high temperature: Electrons, phonons, and the Wiedemann-Franz law. *Phys. Rev.* **2010**, *82*, 75418. [[CrossRef](#)]
82. Dehkordi, A.M.; Zebarjadi, M.; He, J.; Tritt, T.M. Thermoelectric power factor: Enhancement mechanisms and strategies for higher performance thermoelectric materials. *Mater. Sci. Eng. Rep.* **2015**, *97*, 1–22. [[CrossRef](#)]